JMEPEG (2012) 21:1620–1636
DOI: 10.1007/s11665-011-0098-7

1059-9495/$19.00

THz Dielectric Properties of Molecular Clusters of PETN and TNT Calculated by Density Functional Theory

L. Huang, A. Shabaev, S.G. Lambrakos, and L. Massa

(Submitted November 29, 2011)

The need for better detection of explosive devices has imposed a necessity for determining the dielectric response properties of energetic materials with respect to electromagnetic wave excitation. Among the range of different frequencies for electromagnetic excitation, the THz frequency range is of particular interest because of its nondestructive nature. The present study is based on significant progress in density functional theory (DFT), and associated software technology, which is sufficiently mature for the determination of dielectric response functions, and actually provides complementary information to that obtained from experiment. This point is further demonstrated in this study by calculations of ground state resonance structure associated with molecular clusters of the high explosives PETN and TNT using DFT, which is for the construction of parameterized dielectric response functions for excitation by electromagnetic waves at frequencies within the THz range. These dielectric functions provide for different types of analyses concerning the dielectric response of explosives. In particular, these dielectric response functions provide quantitative initial estimates of spectral response features for subsequent adjustment with respect to additional information such as laboratory measurements and other types of theory-based calculations. With respect to qualitative analysis, these spectra provide for the molecular level interpretation of response structure. The DFT software GAUSSIAN was used for the calculations of ground state resonance structure presented here.

Keywords advanced characterization, chemical analysis, modeling processes

1. Introduction

A quantitative understanding of the dielectric response properties of high explosives with respect to electromagnetic wave excitation was motivated in the past by the need for monitoring munitions stockpiles under control of the US Navy, as well as other defense-related organizations. This was necessary because stored explosives are typically characterized by shelf lives and tend to degrade with time, as well as being subjected to environmental influences associated with storage, which can contribute to either their degradation or instability. In addition to understanding the dielectric response of individual explosives, as pure systems, it was necessary to understand their dielectric response as a component of a layered composite material. This was necessary because many explosives, as those used in practice, are a composite of binding materials, purpose of which can be both chemical and structural. It follows that, in the past, a primary motivation for quantitative understanding of dielectric properties of high explosives was for the purpose of accessing performance of energetic materials. The current need for better detection of explosive devices, however, has imposed a new motivation for quantitative understanding of dielectric response properties of high explosives with respect to electromagnetic wave excitation. The motivation for this study is the aim of better detecting improvised explosive devices (IEDs), which is in contrast to the aim of better accessing the performance of materials used in industrially fabricated explosives for the purpose of munitions.

Among the range of different frequencies for electromagnetic excitation, for the purpose of IED detection, the THz frequency range is of particular interest because of its nondestructive nature and ability to penetrate materials that are characteristic of clothing. Typically, the dielectric response properties for electromagnetic wave excitation at THz frequencies, as well as at other frequencies, are determined by means of experimental measurements. The present study is based on significant progress in density functional theory (DFT), and associated software technology, which is sufficiently mature for the determination of dielectric response functions, and actually provides complementary information to that obtained from experiment. In particular, these dielectric response functions provide quantitative initial estimates of spectral response features that can be adjusted with respect to additional information, such as laboratory measurements and other types of theory-based calculations, as well as providing for the molecular level interpretation of response structure.

DFT has been successfully used to investigate the vibrational spectra of energetic materials in the form of single molecules and molecular crystals (Ref 1-7). These calculations provide detection signatures for various forms of materials, which can be encountered in various detection scenarios (Ref 8, 9). The isolated-molecule simulation results help identifying intramolecular vibrational modes in the absorption spectra of various materials. A series of studies have focused on the

L. Huang and **S.G. Lambrakos**, Naval Research Laboratory, Washington, DC 20375; **A. Shabaev**, George Mason University, Fairfax, VA 22030; and **L. Massa**, Hunter College, CUNY, New York, NY. Contact e-mail: lambrakos@anvil.nrl.navy.mil.

general concept of constructing dielectric response functions using DFT for the purpose of quantitative simulation of explosives detection scenarios (Ref 9-11). As emphasized in these studies, the construction of permittivity functions using DFT calculations defines a general approach where dielectric response is estimated within the bounds of relatively well-defined adjustable parameters. Following this approach, permittivity functions are constructed using DFT-calculated absorption spectra under the condition that the calculated resonance locations are fixed, while resonance widths and number densities are assumed adjustable with respect to additional information such as experimentally observed spectra.

Previous studies (Ref 9-11), of which this study is a continuation, considered the calculation of ground state resonance structure associated with single isolated molecules of various high explosives. With respect to practical application, these calculations are relevant for construction of dielectric response functions for detector designs where explosives tend to be in either gas phase or distributed over a surface as single molecules. In what follows, calculations are presented of ground state resonance structure associated with molecular clusters of PETN and TNT. It is significant to note that, with respect to practical application, molecular clusters represent a separate regime for using DFT calculations for construction of dielectric response functions. This regime is intermediate between that of single isolated molecules and molecules making up a crystal lattice. With respect to practical applications, i.e., detector design, this regime is significant in that a wide range of explosive materials are composite materials, which consist of distributions of embedded molecular clusters. Accordingly, the dielectric response functions for these materials, to be adopted for detector design, are weighted averages of the dielectric responses of noninteracting molecular clusters of explosives and the host material within which the clusters are embedded. In addition, with respect to theoretical understanding, the dielectric response of clusters provides insight concerning the nature of the transition of dielectric response to that of solids or systems having long-range order. This type of insight can in turn assist in understanding the nature of the difference between the intermolecular and intramolecular vibrations.

A significant aspect of using response spectra calculated by DFT, for the direct construction of dielectric response functions is that it adopts the perspective of computational physics, according to which a numerical simulation represents another source of ''experimental'' data. This perspective is significant in that a general procedure may be developed for construction of dielectric response functions using DFT calculations as a quantitative initial estimate of spectral response features for subsequent adjustment with respect to additional information such as experimental measurements and other types of theory-based calculations. That is to say, for the purpose of simulating many electromagnetic response characteristics of materials, DFT is sufficiently mature for the purpose of generating data complementing, as well as superseding, experimental measurements.

In the case of THz excitation of materials, the procedure of using response spectra calculated using DFT, which is associated with ground state resonance structure, for the direct construction of permittivity functions is well posed owing to the physical characteristic of THz excitation. In particular, it is important to note that the procedure for constructing a permittivity function using response spectra calculated using DFT is physically consistent with the characteristically linear response associated with THz excitation of molecules. Accordingly, one observes a correlation between the advantages of using THz excitation for detection of explosives (and ambient materials) and those for its numerical simulation based on DFT. Specifically, THz excitation is associated with frequencies that are characteristically perturbative to molecular states, in contrast to frequencies that can induce appreciable electronic state transitions. Of course, the practical aspect of the perturbative character of THz excitation for detection is that detection methodologies can be developed, which do not damage materials under examination. The perturbative character of THz excitation with respect to molecular states has significant implications with respect to its numerical simulation based on DFT. It follows then that, owing to the perturbative character of THz excitation, which is characteristically linear, one is able to make a direct association between local oscillations about ground-state minima of a given molecule and THz excitation spectra.

Construction of permittivity functions according to the best fit of available data for a given material corresponding to different types of experimental measurements has been typically the dominant approach. This approach is extended by using DFT calculations of electromagnetic response as data for construction of permittivity functions. The inclusion of this type of information is significant for accessing what spectral response features at the molecular level are actually detectable with respect to a given set of detection parameters. Accordingly, permittivity functions having been constructed using DFT calculations provide a quantitative correlation between macroscopic material response and molecular structure. Within this context, it is not important that the permittivity function be quantitatively accurate for the purpose of being adopted as input for system simulation. Rather, it is important that the permittivity function be qualitatively accurate in terms of specific dielectric response features for the purpose of sensitivity analysis, which is relevant for the assessment of absolute detectability of different types of molecular structure with respect to a given set of detection parameters. That is to say, permittivity functions that have been determined using DFT can provide a mechanistic interpretation of material's response to electromagnetic excitation that could establish the well posedness of a given detection methodology for detection of specific molecular characteristics. Within the context of practical application, permittivity functions having been constructed according to the best fit of available data would be ''correlated'' with those obtained using DFT for proper interpretation of permittivity-function features. Subsequent to establishment of good correlation between DFT and experiment, DFT calculations can be adopted as constraints for the purpose of constructing permittivity functions, features of which are consistent with molecular level response, for adjustment relative to specific sets of either experimental data or additional molecular level information.

In what follows, calculations are presented of ground state resonance structure associated with molecular clusters of PETN and TNT, which is for the construction of parameterized dielectric response functions for excitation by electromagnetic waves at compatible frequencies. For this purpose, the DFT software GAUSSIAN09 (G09) was adopted (Ref 12).

The organization of the subject areas presented here are as follows. First, a brief description of the elements of vibrational analysis using DFT relevant for the calculation of absorption spectra is presented. Second, a general review is presented concerning the formal structure of permittivity functions in

terms of analytic function representations. An understanding of the formal structure of permittivity functions in terms of both physical consistency and causality is important for post-processing of DFT calculations for the purpose of constructing permittivity functions. Third, information concerning the ground state resonance structure of molecular clusters of PETN and TNT, which is obtained using DFT, is presented. This information consists of the ground state molecular geometry and response spectrum for single isolated molecule and molecular clusters of PETN and TNT. Fourth, a discussion is presented that elucidates the utility of information concerning the ground state resonance structure of molecular clusters of explosives. This discussion also suggests procedures for the construction of permittivity functions that are in terms of reduced sets of phenomenological parameters. Finally, a conclusion is given summarizing the significance of modeling the dielectric response of molecular clusters relative to explosives detection in practice.

2. Construction of Dielectric Response Functions Using DFT

As in previous studies (Ref 9-11), the formal mathematical structure underlying DFT calculations, as well as the procedure for constructing permittivity functions using these calculations, is included here for purposes of completeness. A brief description of this mathematical structure is as follows.

The DFT software GAUSSIAN09 (G09) can be used to compute an approximation of the IR absorption spectrum of a molecule or molecules (Ref 12). This program calculates vibrational frequencies by determining second derivatives of the energy with respect to the Cartesian nuclear coordinates, and then transforming to mass-weighted coordinates at a stationary point of the geometry (Ref 13). The IR absorption spectrum is obtained using DFT to compute the ground state electronic structure in the Born-Oppenheimer approximation using Kohn-Sham density functional theory (Ref 14-18). GAUSSIAN uses specified orbital basis functions to describe the electronic wavefunctions and density. For a given set of nuclear positions, the calculation directly gives the electronic charge density of the molecule, the potential energy V, and the displacements in Cartesian coordinates of each atom. The procedure for vibrational analysis followed in GAUSSIAN is that described in Ref 19. Reference 20 presents a fairly detailed review of this procedure. A brief description of this procedure is as follows.

The procedure followed by GAUSSIAN is based on the fact that the vibrational spectrum depends on the Hessian matrix $\mathbf{f}_{\mathrm{CART}}$, which is constructed using the second partial derivatives of the potential energy V with respect to displacements of the atoms in Cartesian coordinates. Accordingly, the elements of the $3N \times 3N$ matrix $\mathbf{f}_{\mathrm{CART}}$ are given by

$$f_{\mathrm{CART}ij} = \left(\frac{\partial^2 V}{\partial \xi_i \partial \xi_j}\right)_0 \qquad \text{(Eq 1)}$$

where $\{\xi_1, \xi_2, \xi_3, \xi_4, \xi_5, \xi_6, \ldots, \xi_{3N}\} = \{\Delta x_1, \Delta y_1, \Delta z_1, \Delta x_2, \Delta y_2, \Delta z_2, \ldots, \Delta z_N\}$, which are displacements in Cartesian coordinates, and N is the number of atoms. As discussed above, the zero subscript in Eq 1 indicates that the derivatives are taken at the equilibrium positions of the atoms, and that the first derivatives are zero. Given the Hessian matrix defined by Eq 1, the operations for calculation of the vibrational spectrum require that the Hessian matrix Eq 1 be transformed to mass-weighted Cartesian coordinates according to the relation

$$f_{\mathrm{MWC}ij} = \frac{f_{\mathrm{CART}ij}}{\sqrt{m_i m_j}} = \left(\frac{\partial^2 V}{\partial q_i \partial q_j}\right)_0 \qquad \text{(Eq 2)}$$

where $\{q_1, q_2, q_3, q_4, q_5, q_6, \ldots, q_{3N}\} = \{\sqrt{m_1}\Delta x_1, \sqrt{m_1}\Delta y_1, \sqrt{m_1}\Delta z_1, \sqrt{m_2}\Delta x_2, \sqrt{m_2}\Delta y_2, \sqrt{m_2}\Delta z_2, \ldots, \sqrt{m_N}\Delta z_N\}$ are the mass-weighted Cartesian coordinates. GAUSSIAN computes the energy second derivatives Eq 2, thus computing the forces for displacement perturbations of each atom along each Cartesian direction. The first derivatives of the dipole moment with respect to atomic positions $\partial\vec{\mu}/\partial\xi_i$ are also computed. Each vibrational eigenmode leads to one peak in the absorption spectrum, at a frequency equal to the mode's eigenfrequency ν_{n0}. The absorption intensity corresponding to a particular eigenmode n eigenfrequency of which is ν_{n0} is given by

$$I_n = \frac{\pi}{3c}\left|\sum_{i=1}^{3N} \frac{\partial\vec{\mu}}{\partial\xi_i} l_{\mathrm{CART}in}\right|^2, \qquad \text{(Eq 3)}$$

where $\mathbf{l}_{\mathrm{CART}}$ is the matrix elements of which are the displacements of the atoms in Cartesian coordinates. The matrix $\mathbf{l}_{\mathrm{CART}}$ is determined by the following procedure. First,

$$\mathbf{l}_{\mathrm{CART}} = \mathbf{M}\mathbf{l}_{\mathrm{MWC}}, \qquad \text{(Eq 4)}$$

where $\mathbf{l}_{\mathrm{MWC}}$ is the matrix elements of which are the displacements of the atoms in mass-weighted Cartesian coordinates, and $\mathbf{M}$ is a diagonal matrix defined by the elements

$$M_{ii} = \frac{1}{\sqrt{m_i}}. \qquad \text{(Eq 5)}$$

Proceeding further, $\mathbf{l}_{\mathrm{MWC}}$ is the matrix needed to diagonalize $\mathbf{f}_{\mathrm{MWC}}$ defined by Eq 2 such that

$$(\mathbf{l}_{\mathrm{MWC}})^{\mathrm{T}}\mathbf{f}_{\mathrm{MWC}}(\mathbf{l}_{\mathrm{MWC}}) = \Lambda, \qquad \text{(Eq 6)}$$

where Λ is the diagonal matrix with eigenvalues λ_i. The procedure for diagonalizing Eq 6 consists of the operations:

$$\mathbf{f}_{\mathrm{INT}} = (\mathbf{D})^{\mathrm{T}}\mathbf{f}_{\mathrm{MWC}}(\mathbf{D}) \qquad \text{(Eq 7)}$$

and

$$(\mathbf{L})^{\mathrm{T}}\mathbf{f}_{\mathrm{MWC}}(\mathbf{L}) = \Lambda, \qquad \text{(Eq 8)}$$

where $\mathbf{D}$ is a matrix transformation to coordinates where rotation and translation have been separated out, and $\mathbf{L}$ is the transformation matrix composed of eigenvectors calculated according to Eq 8. The eigenfrequencies in units of (cm^{-1}) are calculated using the eigenvalues: λ_n by the expression

$$\nu_{n0} = \frac{\sqrt{\lambda_n}}{2\pi c}, \qquad \text{(Eq 9)}$$

where c is the speed of light. The elements of $\mathbf{l}_{\mathrm{CART}}$ are given by

$$l_{\mathrm{CART}ki} = \sum_{j=1}^{3N} \frac{D_{kj}L_{ji}}{\sqrt{m_j}}, \qquad \text{(Eq 10)}$$

where k, i = 1, …, $3N$, and the column vectors of these elements are the normal modes in Cartesian coordinates.

The intensity Eq 3 must then be multiplied by the number density of molecules to give an absorption strength. It follows that the absorption spectrum calculated by GAUSSIAN is a sum of delta functions, positions and magnitudes of which correspond to the vibrational frequencies and magnitudes, respectively. In principle, however, these spectral components must be broadened and shifted to account for anharmonic effects such as finite mode lifetimes and inter-mode couplings.

The construction of permittivity functions using DFT calculations requires that a specific parametric function representation be adopted. This parametric representation must be physically consistent with specific molecular response characteristics, while limiting the inclusion of feature characteristics that tend to mask response signatures that may be potentially detectable. In principle, parameterizations are of two classes. One class consists of parameterizations that are directly related to molecular response characteristics. This class of parameterizations would include spectral scaling and width coefficients. The other class consists of parameterizations that are purely phenomenological and are structured for optimal and convenient best fits to experimental measurements. A sufficiently general parameterization of permittivity functions is given by the Drude-Lorentz approximation (Ref 21, 22)

$$\varepsilon(\nu) = \varepsilon'(\nu) + i\varepsilon''(\nu) = \varepsilon_\infty + \sum_{n=1}^{N} \frac{\nu_{np}^2}{(\nu_{n0}^2 - \nu^2) - i\gamma_n \nu}, \quad \text{(Eq 11)}$$

where ν_{np} and γ_n are the spectral scaling and width of a resonance contributing to the permittivity function. The permittivity ε_∞ is a constant since the dielectric response at high frequencies is substantially detuned from the probe frequency. The real and imaginary parts, $\varepsilon_r(\nu)$ and $\varepsilon_i(\nu)$, respectively, of the permittivity function can be written separately as

$$\varepsilon_r(\nu) = \varepsilon_\infty + \sum_{n=1}^{N} \frac{\nu_{np}^2(\nu_{n0}^2 - \nu^2)}{(\nu_{n0}^2 - \nu^2)^2 + \gamma_n^2\nu^2} \quad \text{and}$$

$$\varepsilon_i(\nu) = \sum_{n=1}^{N} \frac{\nu_{np}^2 \gamma_n \nu}{(\nu_{n0}^2 - \nu^2)^2 + \gamma_n^2\nu^2}. \quad \text{(Eq 12)}$$

With respect to practical application, the absorption coefficient α and index of refraction n_r, given by

$$\alpha = \frac{4\pi\nu}{\sqrt{2}}\left[-\varepsilon_r + \sqrt{\varepsilon_r^2 + \varepsilon_i^2}\right]^{1/2} \quad \text{and}$$

$$n_r = \frac{1}{\sqrt{2}}\left[\varepsilon_r + \sqrt{\varepsilon_r^2 + \varepsilon_i^2}\right]^{1/2}, \quad \text{(Eq 13)}$$

respectively, provide direct relationships between calculated quantities obtained by DFT and the "conveniently measurable" quantities α and n_r. It is significant to note that in what follows, the absorption coefficient α is determined using DFT-calculated spectra in the same spirit as for its measurement in the laboratory. Although permittivity functions $\varepsilon(\nu)$ are not determined explicitly in the present study, it must be kept in mind that the ultimate construction of these functions is necessary for using DFT-calculated spectra to model the dielectric response of complex composite materials and associated detector designs (Ref 9).

3. Ground State Resonance Structure of Three-Molecule Cluster of PETN

In this section are presented the results of computational experiments using DFT concerning a three-molecule cluster of PETN. These results include the relaxed or equilibrium configuration of a single isolated molecule of PETN (see Table 1) and ground-state oscillation frequencies and IR intensities for this configuration, which are calculated by DFT according to the frozen phonon approximation (see Table 2). The ground state resonance structure for a single isolated molecule of PETN is adopted as a reference for analysis of spectral features associated with a three-molecule cluster. For these calculations, geometry optimization and vibrational analysis was effected using the DFT model B3LYP (Ref 23, 24) and basis function 6-311G(2d,2p) (Ref 25, 26). According to the specification of this basis function, (2d,2p) designates polarization functions having 2 sets of d functions for heavy atoms and 2 sets of p functions for hydrogen atoms (Ref 27). A schematic representation of the molecular geometry of a single isolated molecule of PETN is shown in Fig. 1. A schematic representation of the molecular geometry of molecular cluster consisting of 3 molecules is shown in Fig. 2. It is significant to note that the relative positions of the molecules associated with this molecular cluster are according to crystallographic structure conditions that would be associated with bulk material. The ground-state oscillation frequencies and IR

Table 1 Atomic positions of PETN (Å) after optimization

Atomic number	*X*	*Y*	*Z*
6	−0.89008	0.487044	0.169443
6	0.56833	0.025631	0.355901
6	−0.954153	2.010353	0.393203
6	−1.775405	−0.266852	1.180709
6	−1.399001	0.17896	−1.25209
8	−0.536524	2.246621	1.753563
8	0.594489	−1.388358	0.071682
8	−3.114945	0.243543	1.019535
8	−0.503707	0.845656	−2.165744
8	−5.169236	0.102355	1.756224
8	−3.660475	−1.176108	2.678384
8	−0.213539	3.790051	3.268901
8	−0.916392	4.418249	1.301021
8	−0.065066	1.202636	−4.278301
8	−1.784867	−0.046988	−3.786458
8	1.885603	−3.148164	−0.06536
8	2.801652	−1.246607	0.487954
1	−1.969444	2.373078	0.253141
1	−0.289344	2.531375	−0.29121
1	0.903906	0.201954	1.374781
1	1.224466	0.550575	−0.333979
1	−1.43301	−0.084138	2.196278
1	−1.763653	−1.336176	0.985073
1	−2.410743	0.55161	−1.391197
1	−1.382201	−0.89204	−1.438315
7	−4.069163	−0.341502	1.911776
7	−0.561634	3.625752	2.13612
7	1.895046	−1.976796	0.177844
7	−0.825239	0.640236	−3.54537

Table 2 Oscillation frequencies and IR intensities for single isolated molecule of PETN

Frequency, cm^{-1}	Intensity, km/mol
23.0186	0
23.468	1.7622
37.0668	0.0792
38.2553	1.0181
38.256	1.0182
49.1445	0
51.2098	0.0198
56.1273	1.4445
56.1281	1.4444
125.0831	0.5041
125.0838	0.5041
137.2362	0.8057
149.3	0
175.381	0
198.2257	0.822
198.2262	0.822
213.1381	0
253.3021	2.0613
256.0704	1.9542
256.0709	1.9542
309.178	1.5099
319.7365	0
453.5805	3.6627
453.5809	3.6627
533.9816	12.509
589.553	0
620.4669	9.0561
625.7476	8.654
625.7479	8.6542
676.3956	0
711.7268	53.505
711.7271	53.5047
756.1322	54.9232
775.0616	12.1352
775.0623	12.1353
775.6437	0
776.5314	30.3068
842.7866	0
857.2537	365.5689
857.2545	365.5689
861.1535	708.764
887.0866	0
927.126	12.2082
944.6012	7.5925
944.6018	7.5925
1015.2359	0
1031.1128	68.9949
1031.1133	68.9954
1063.903	0
1069.3729	100.3831
1184.1914	2.4068
1203.243	0.1994
1203.2433	0.1994
1264.3964	0
1284.5981	21.2105
1284.5988	21.2112
1310.0272	243.6025
1329.7418	272.2731
1329.7419	272.2725
1343.2953	0
1344.2228	196.2847
1406.7094	43.0983
1406.7097	43.0982
1410.9192	64.19
1425.4355	0
1513.7205	0
1514.457	4.0158
1520.2629	13.4384
1520.2631	13.4385
1765.1326	0
1766.3812	231.1996
1767.5533	544.1035
1767.554	544.1009
3081.5559	5.7489
3082.5044	7.1942
3082.5051	7.1942
3084.4409	0
3139.0088	0
3140.7324	5.4891
3140.7327	5.4894
3143.0876	10.9428

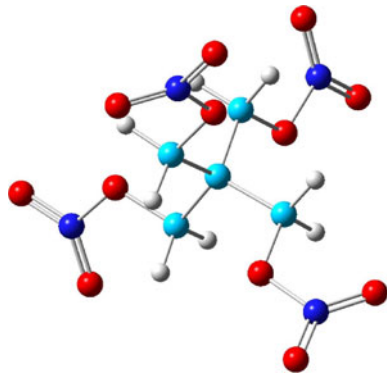

Fig. 1 Molecular geometry of PETN

intensities for the three-molecule cluster of PETN, corresponding to its relaxed equilibrium configuration, are calculated by DFT according to the frozen phonon approximation. In the case of a molecular cluster of 3 molecules, these values are given in Table 3. The DFT model and basis function used for these calculations are the same used for the single isolated molecule of PETN. Two programs, ConQuest and Mercury (Ref 28), have been used for searching the Cambridge Structural Database (CSD), visualizing database entries for PETN (and TNT in what follows), and for creating the *n*-molecule clusters. When constructing the cluster it was necessary to consider the interactions and forces between the single molecule and its intermolecular neighborhood. In particular, a consideration of hydrogen bonding between the molecules is important for establishing the cluster.

Proceeding further, shown in Fig. 3 and 4 are the calculated IR intensities for a single isolated molecule and three-molecule cluster of PETN. The IR intensities shown in these figures are given in the form of discrete delta-function representations of the spectra. Comparison of these figures shows a noticeable increase in the number of resonances for the molecular cluster relative to the single molecule. This increase is physically consistent with the manifestation of resonant modes associated

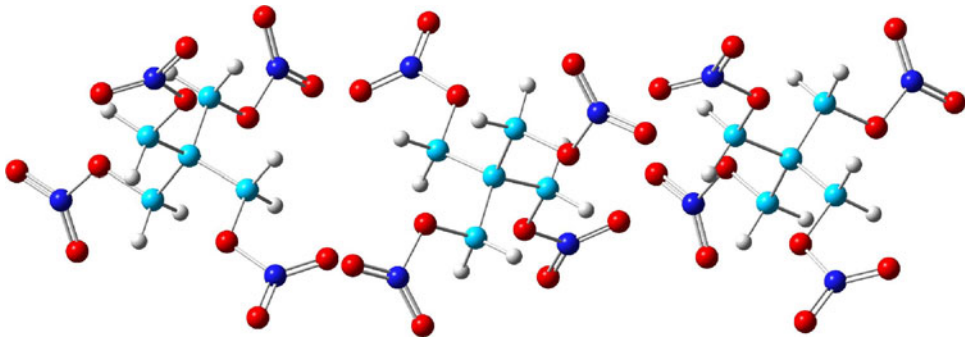

Fig. 2 Molecular geometry of three-molecule cluster of PETN

Table 3 Oscillation frequencies and IR intensities for three-molecule cluster of PETN

Frequency, cm^{-1}	Intensity, km/mol
2.7459	0.005
3.0959	0
5.9927	0
9.3696	0.0003
9.4769	0.0102
12.6516	0.0555
19.0972	0.6809
21.5863	0.0499
23.4909	3.1816
24.2182	0.0223
24.2957	0.1038
26.1885	0.0298
27.792	0.0928
29.53	0.6686
32.3744	0.148
33.728	0.6131
36.5112	0.1353
37.9722	1.142
40.1106	0.1238
40.2686	0.7434
40.6739	0.0067
41.148	0.0902
45.3709	0.8009
45.4139	0.0058
49.0572	0.1161
52.0377	0.0004
52.0415	2.3979
52.8558	0.211
54.4623	4.7351
56.9478	1.8936
56.9559	0.0156
58.1967	0.8009
59.0884	0.0242
60.7896	0.0144
62.0465	2.6393
64.1165	0.017
67.5021	2.5334
81.1563	0.063
82.4234	0.2897
123.768	1.6121
123.9862	0.0784
125.3659	0.059
129.7586	0.995
129.8118	0.2058
140.6045	1.3884
140.8086	0.7455
141.5511	0.6157
143.6774	0.09

Table 3 Continued

Frequency, cm^{-1}	Intensity, km/mol
150.8196	0
151.0548	0.6581
151.6617	0
179.9747	0.0565
179.9893	0.091
187.9166	0.0943
191.0116	1.1948
193.9818	4.2534
193.9882	0.0045
203.0462	1.4143
203.1005	0.0342
204.4253	0.2964
215.1988	0.0063
215.2201	0.0489
216.7523	0.0112
253.5204	2.5784
253.5395	1.3166
255.4469	2.9787
256.9556	4.6241
256.9622	0.0114
258.4687	2.3891
260.5664	0.4464
260.6916	6.0475
261.354	4.6746
308.4312	0.5996
310.0498	1.3298
310.2897	5.5818
318.7477	0.0604
319.4577	0.5603
319.48	0.2014
452.9283	7.3557
452.9482	0.3582
454.1579	3.0692
456.9975	9.8235
457.2185	0.0887
458.9726	1.6145
535.0382	21.8539
535.0643	0.3361
536.2878	2.4334
590.701	0.0464
590.7104	0.044
591.5033	0.0049
621.6932	9.3787
621.7182	2.4644
623.7837	6.7643
624.7261	0.1423
625.2445	1.4605
625.2576	16.8618
630.3136	20.158

Table 3 Continued

Frequency, cm^{-1}	Intensity, km/mol
630.4765	2.2566
633.2105	21.9922
677.9521	2.6767
677.9772	0.5639
679.5992	1.3293
711.3558	37.4622
711.5214	0.0131
711.6724	135.8772
714.8454	67.0988
714.9153	4.0388
717.5967	55.4965
754.8807	8.6665
755.7139	6.5923
755.9681	125.2554
771.4876	35.9297
771.5766	0.5576
772.0193	52.9692
772.045	32.2983
775.0159	0.3922
775.0287	17.1464
775.3692	5.8581
775.3761	7.2323
775.5979	15.9024
776.2775	20.1457
776.3102	0.0334
776.7685	18.1673
843.0367	11.9947
843.3959	10.8952
844.2677	3.2431
852.5711	74.5096
854.7542	1.2119
855.0319	1113.0496
859.1821	440.0582
859.2446	328.521
862.1922	204.4109
867.808	188.3015
870.1517	767.9538
872.9782	442.748
890.1616	10.2077
891.835	78.6084
896.2267	265.5877
928.7986	20.8334
928.7987	0.2006
931.284	22.9396
939.29	0.062
942.0798	0.9418
942.9281	15.3538
948.6176	15.6586
948.6245	2.9713
950.0091	9.2565
1013.7078	0.5689
1014.4844	1.6776
1014.6168	1.0282
1021.6065	38.8561
1026.3538	0.189
1026.4937	140.2393
1033.9843	152.6453
1034.1356	0.5469
1036.3997	108.9989
1060.5533	11.1806
1063.3865	1.689
1063.7787	52.3445
1068.8099	46.4614
1069.15	1.7564
1070.5229	152.8388

Table 3 Continued

Frequency, cm^{-1}	Intensity, km/mol
1182.1937	0.5315
1183.4821	0.5997
1183.5236	3.8764
1200.4976	0.5446
1201.5612	1.1979
1201.5688	0.0735
1203.6359	0.3577
1203.7332	0.0599
1203.8767	0.012
1264.6515	0.0131
1264.6724	1.2153
1264.6882	0
1284.3719	71.0302
1284.4592	0.0881
1284.9974	15.2172
1287.3538	49.0979
1287.3636	0.2869
1289.071	24.2026
1308.4966	10.5086
1310.3143	22.3865
1312.6071	576.5331
1324.9568	463.472
1326.1389	650.3981
1328.1746	0.0026
1330.5981	0.0236
1331.6897	357.7667
1332.6163	325.2102
1341.1545	0.0623
1342.6538	0.8549
1343.0424	2.8398
1344.1932	3.4047
1344.3925	9.4586
1344.9041	489.2351
1407.7294	75.5986
1407.7589	0.0147
1408.5706	80.8585
1408.7397	11.8525
1408.9039	56.6913
1410.5243	34.4459
1412.4119	12.556
1412.4762	67.0457
1413.4799	85.1998
1426.6968	0.2855
1426.7509	1.5948
1427.8077	0.8237
1504.132	2.0613
1506.4666	40.4544
1508.4739	0.522
1511.4553	16.212
1512.9001	0.4156
1513.5698	2.3789
1513.6084	1.62
1516.7607	3.007
1516.7999	16.3591
1518.0491	10.1118
1519.4949	21.3927
1519.5026	0.0019
1746.3506	1019.5118
1746.6143	236.3832
1752.1338	0.2487
1753.121	121.7147
1766.1827	656.7066
1766.2982	0.0164
1766.9027	527.3882
1767.3317	131.9252

Table 3 Continued

Frequency, cm^{-1}	Intensity, km/mol
1768.5984	63.6771
1769.1071	244.2138
1770.5093	937.002
1770.6707	151.094
3078.3787	9.9733
3078.3806	3.0626
3079.4727	12.1956
3079.8242	1.1214
3081.5474	8.191
3081.5496	2.1684
3083.6433	13.4875
3083.6489	0.0252
3095.5657	10.7196
3096.1804	2.0796
3098.1538	3.8464
3098.1646	1.7708
3136.0608	5.0163
3136.0637	3.8842
3140.5251	5.7739
3140.7388	9.6767
3140.7444	0.0509
3140.7461	5.9203
3147.1145	6.1931
3147.1213	5.1318
3155.8755	4.9167
3156.3723	4.0165
3160.1804	3.5558
3160.1809	5.7426

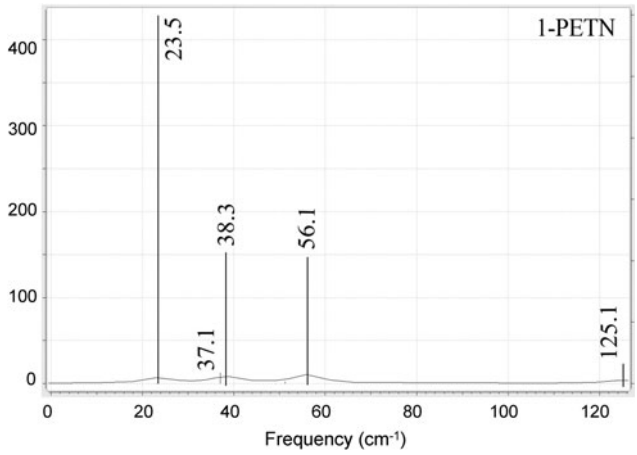

Fig. 3 IR intensity (arbitrary units) as a function of frequency calculated using DFT B3LYP/6-311G(2d,2p) for single isolated molecule of PETN according to frozen phonon approximation

with intermolecular coupling within the molecular cluster. Shown in Fig. 5 and 6 are continuous spectra that are constructed using a superposition of essentially Lorenzian functions of various heights and widths, which have been fit to the discrete spectra given in Table 2 and 3, respectively. This construction is applied within the GAUSSIAN program (Ref 12). The significance of this type of construction is discussed further below. Comparison of Fig. 5 and 6 shows the persistence of various dominant resonance signatures for both a

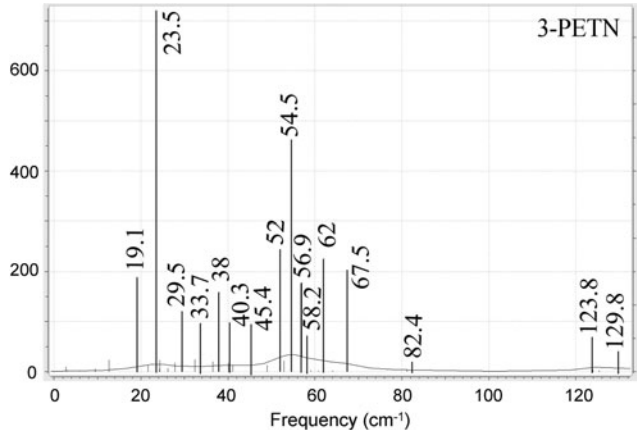

Fig. 4 IR intensity (arbitrary units) as a function of frequency calculated using DFT B3LYP/6-311G(2d,2p) for three-molecule cluster of PETN according to frozen phonon approximation

single isolated molecule and molecular cluster. This result supports the notion as suggested in previous studies (Ref 10, 11) that permittivity functions constructed using DFT-calculated spectra for single isolated molecules may be sufficient for detection in cases of excitation frequencies compatible with intramolecular resonance modes.

4. Ground State Resonance Structure of Molecular Clusters of TNT

In this section are presented the results of computational experiments using DFT concerning molecular clusters of TNT. These results include the relaxed or equilibrium configuration of a single isolated molecule of TNT (see Table 4) and ground-state oscillation frequencies and IR intensities for this configuration, which are calculated by DFT according to the frozen phonon approximation (see Table 5). The ground state resonance structure for a single isolated molecule of TNT is adopted as a reference for analysis of spectral features associated with molecular clusters of different sizes. For these calculations, geometry optimization and vibrational analysis was effected using the same DFT model and basis function 6-311G(2d,2p) used for PETN presented above. A schematic representation of the molecular geometry of a single isolated molecule of TNT is shown in Fig. 7. A schematic representation of molecular geometries of molecular clusters consisting of 2 and 4 molecules are shown in Fig. 8 and 9, respectively. It is significant to note that the relative positions of the molecules associated with each of the molecular clusters is according to crystallographic structure conditions that would be associated with bulk material. The ground-state oscillation frequencies and IR intensities for the different molecular clusters of TNT, corresponding to their relaxed equilibrium configurations, are calculated by DFT according to the frozen phonon approximation. In the cases of molecular clusters of 2 and 4 molecules, these values are given in Table 6 and 7, respectively. As in the case of PETN presented above, the DFT model and basis function used for these calculations are the same as those used for the single isolated molecule of TNT.

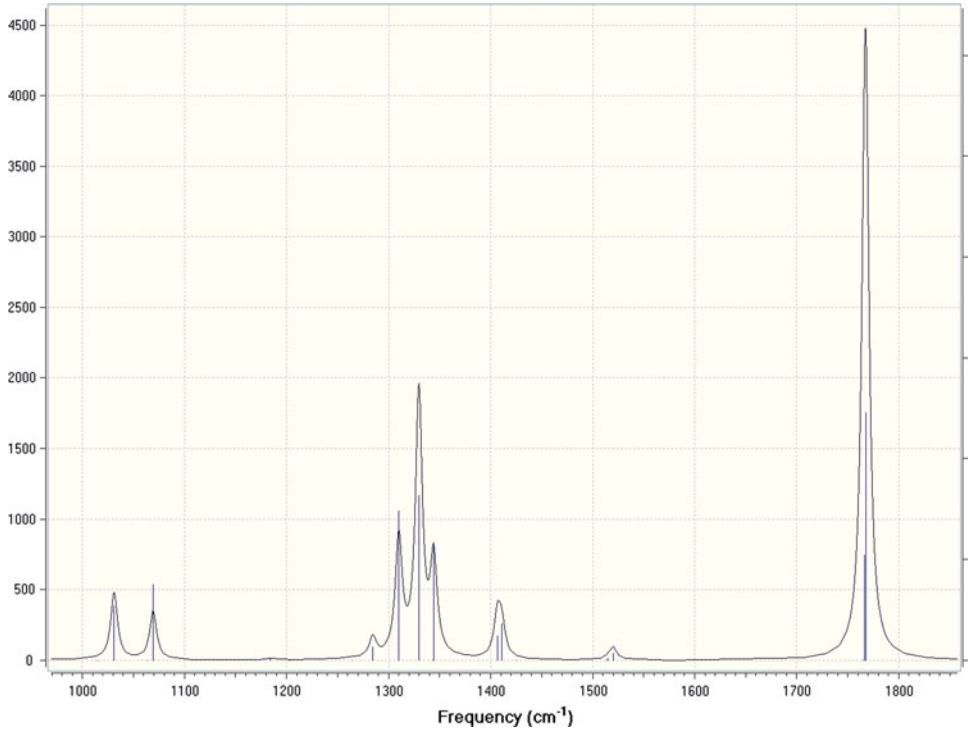

Fig. 5 Continuous-spectrum representation of IR intensity (arbitrary units) as a function of frequency calculated using DFT for single isolated molecule of PETN

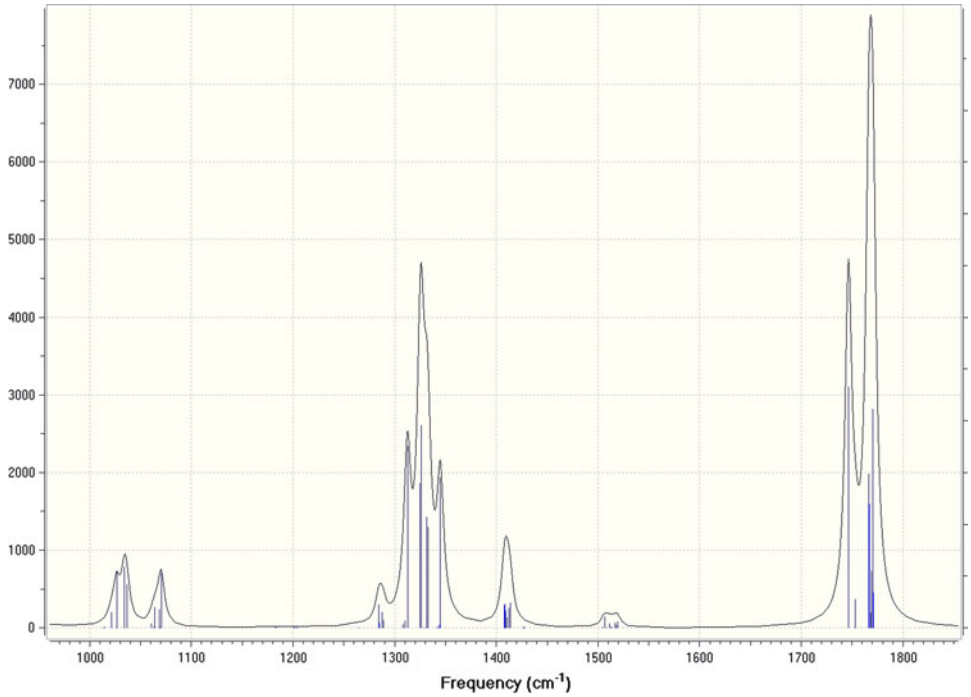

Fig. 6 Continuous-spectrum representation of IR intensity (arbitrary units) as a function of frequency calculated using DFT for three-molecule cluster of PETN

Proceeding further, shown in Fig. 10-12 are the calculated IR intensities for a single isolated molecule and molecular clusters consisting of two and four molecules of TNT. Shown in Fig. 13-15, are continuous spectra consisting of a superposition of essentially Lorenzian functions of various heights and widths, which have been constructed using the discrete spectra given in Table 5-7, respectively. Referring to Fig. 10-12, one observes a noticeable increase in the number of resonances with increase in molecular cluster size. Again, this increase is physically consistent with the manifestation of resonant modes

Table 4 Atomic positions for equilibrium configuration of TNT (Å)

Atomic number	*X*	*Y*	*Z*
1	1.294359	−0.627693	1.916458
1	−2.458208	−0.867791	−0.128619
1	0.754635	0.052629	−3.504585
1	1.68668	−1.400164	−3.189867
1	2.304987	0.153675	−2.659394
6	0.730091	−0.664364	0.998736
6	−0.646569	−0.782893	1.016672
6	−1.382696	−0.799534	−0.152696
6	−0.701136	−0.724375	−1.355556
6	0.693755	−0.609698	−1.463028
6	1.364308	−0.592195	−0.229936
6	1.399735	−0.432944	−2.779328
7	−1.347001	−0.883583	2.313715
7	2.841751	−0.500544	−0.177322
7	−1.547799	−0.781608	−2.569596
8	3.474661	−1.155138	−0.992685
8	3.321537	0.203741	0.698298
8	−0.658543	−0.86075	3.323182
8	−2.564711	−0.982781	2.284321
8	−2.607727	−0.174823	−2.533999
8	−1.14092	−1.451907	−3.507164

associated with intermolecular coupling within the molecular cluster, which are at relatively lower frequencies, which are in turn compatible with intermolecular resonance modes. Referring to Fig. 13-15, which in contrast to Fig. 10-12, show spectra at relatively higher frequencies, which are in turn compatible with intramolecular resonance modes, the persistence of various dominant resonance signatures are readily observable.

5. Discussion

The DFT-calculated absorption spectra given in Table 2, 3, and 5-7 provide two types of information for general analysis of dielectric response. These are the denumeration of ground state resonance modes and estimates of molecular level dielectric response structure. The construction of permittivity functions using the DFT-calculated absorption spectra follows the same procedure as that applied for the construction of permittivity functions using experimentally measured absorption spectra, but with the addition of certain constraint conditions. Accordingly, construction of permittivity functions using either DFT or experimentally measured absorption spectra requires parameterizations that are in terms of physically consistent analytic function representations such as the Drude-Lorentz model. Although the formal structure of permittivity functions constructed using DFT and experimental measurements are the same, their interpretation with respect to parameterization is different for each case.

The construction of permittivity functions using experimental measurements defines an inverse problem where resonant locations, peaks and widths, as well as the number of resonances, are assumed adjustable. Following this approach, it follows that many of the detailed characteristics of resonance structure are smoothed or averaged. In addition, measurement

Table 5 Oscillation frequencies and IR intensities for single isolated molecule of TNT

Frequency, cm^{-1}	Intensity, km/mol
48.1344	0.1511
54.4696	0.0031
54.6314	0.449
95.2736	4.9386
120.4472	4.6364
149.4345	2.5947
176.8858	0.2872
187.9397	0.1349
195.623	4.7398
296.0832	1.9743
324.2345	0.2144
327.7225	0.0382
352.9275	2.4697
367.8506	1.3391
386.8114	1.1556
470.7113	1.3672
481.9805	0.0293
541.3526	1.0016
548.7636	2.1862
662.2958	9.245
667.0623	0.0724
717.9113	20.7181
739.4252	51.7192
760.6036	27.3511
790.626	0.2088
797.0792	6.7309
805.7737	11.3147
843.4395	1.7202
919.629	37.1859
951.7191	31.8976
960.2885	2.6521
966.588	10.2579
1046.3734	3.8264
1051.7325	1.107
1093.3557	53.251
1183.9727	9.8852
1208.2366	14.9414
1220.3445	0.256
1354.5992	4.7978
1389.0625	326.8959
1392.5596	309.3893
1402.1146	5.7057
1422.838	4.377
1423.0629	6.7083
1475.6511	2.6229
1479.3087	11.0602
1495.7421	9.6734
1608.9564	75.6162
1626.0082	155.939
1637.3636	7.7795
1668.2966	226.3714
1668.9285	185.4888
3075.5823	0.8369
3143.8171	5.2936
3175.73	4.0642
3256.9297	12.3643
3257.0266	29.788

artifacts associated with sample preparation and detector configuration can in principle introduce errors. One advantage of permittivity functions constructed using experimental measurements, however, is that many aspects of dielectric response on the macroscale that are associated with multiscale averaging

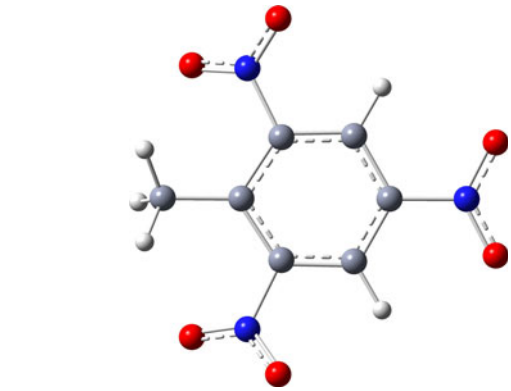

Fig. 7 Molecular geometry of TNT

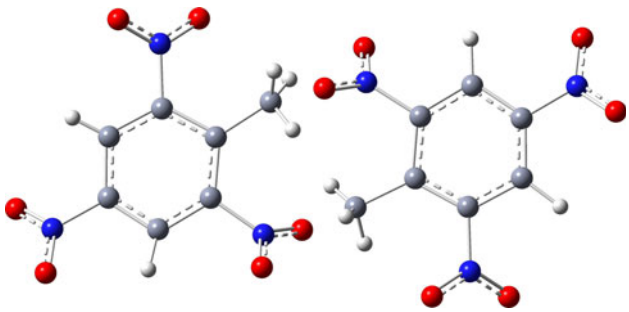

Fig. 8 Molecular geometry of two-molecule cluster of TNT

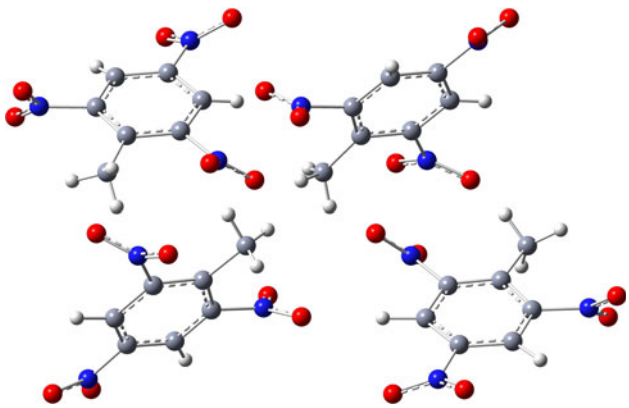

Fig. 9 Molecular geometry of four-molecule cluster of TNT

and molecule-lattice coupling are taken into account inherently. Accordingly, the disadvantage of this approach is that the nature of any multiscale averaging and resonant structure, contributing to dielectric response on the macroscopic level, may not be understood. This lack of quantitative understanding can in principle inhibit the development of pump-probe type methodologies for selective excitation of molecular modes, which are for the purpose of enhanced signature detection or modulation. Better interpretation of dielectric response of explosives on a macroscale can be achieved through correlation of resonance structure, which is experimentally observed, with spectra calculated by DFT. In principle, correlation of resonance structure would include the quantitative analysis of changes in signature features associated with the transition of

Table 6 Oscillation frequencies and IR intensities for two-molecule cluster of TNT

Frequency, cm^{-1}	Intensity, km/mol
8.1269	0.0355
9.2439	0.1381
14.9722	0.1304
17.9857	0.0806
27.8664	0.1452
51.3591	0.1152
52.1877	0.1647
54.9708	0.1831
56.1668	0.0134
59.7929	0.3965
78.491	1.4342
89.0883	0.0858
101.2143	7.358
103.5822	5.1626
123.1052	6.1392
127.3796	3.0096
150.451	3.4095
153.1326	1.5344
179.5611	0.7559
185.8249	1.666
189.4679	0.2125
193.7987	7.0708
194.5187	1.3655
199.9836	2.5218
296.0558	3.3548
296.6949	0.8447
324.7901	0.2067
325.6773	0.2503
326.5354	0.035
329.1659	0.2011
352.9561	1.8829
353.7762	2.7653
367.1677	1.2469
368.4943	1.7859
385.1874	1.5395
387.5417	1.2049
470.4774	0.6591
471.4932	1.4576
482.1479	0.0734
483.016	0.4663
541.2321	0.2644
541.4728	3.0752
548.9486	0.5345
549.1266	5.0519
661.4668	18.0395
662.5497	2.1107
668.0229	0.449
668.7801	0.2078
717.8515	14.8535
718.1848	26.9107
739.2918	111.0234
740.0657	7.4066
760.1704	33.4574
760.7635	22.866
790.55	0.2145
791.5138	0.1071
796.5846	2.8469
796.7956	10.0258
805.9091	21.8258
806.2351	2.4385
843.0377	0.4042
844.2998	3.981
921.465	5.1014
922.0174	62.7738

Table 6 Continued

Frequency, cm^{-1}	Intensity, km/mol
952.5892	34.8719
953.1544	30.8313
959.6472	4.1415
960.2688	2.7507
966.3623	10.1398
966.7785	10.4861
1048.9553	3.3337
1050.6176	4.1689
1052.5814	2.3397
1056.3804	1.6056
1094.1389	39.3235
1094.3667	64.4747
1184.6285	15.6223
1184.7833	4.4717
1208.917	6.8039
1209.2321	26.3875
1220.4561	0.3392
1222.2325	0.3771
1354.3826	15.2785
1355.7351	7.5663
1388.4705	610.8024
1389.1523	31.4292
1392.7549	647.5478
1394.4088	58.375
1402.6722	1.3532
1405.172	40.3744
1421.4177	9.6829
1422.4552	5.9836
1424.182	3.6857
1424.5634	7.0426
1475.9287	9.638
1476.429	0.6661
1477.5623	5.8383
1480.2882	9.2747
1499.3215	7.3228
1501.9449	6.629
1607.2729	14.1997
1608.0475	147.0028
1620.5898	76.0466
1624.0647	230.3202
1633.2048	22.9768
1634.0034	18.3162
1664.0026	50.159
1667.4041	334.8076
1668.4406	210.3268
1669.2795	166.2294
3074.9392	0.8768
3075.6946	0.259
3146.9888	2.6818
3147.3743	4.1554
3180.3569	1.1336
3180.9182	3.7902
3255.7366	23.6929
3257.2678	21.2765
3258.4272	17.8489
3260.5779	14.6354

the system from that of a low-density system of uncoupled molecule to that of a bulk lattice.

One approach for the construction of permittivity functions using DFT calculations, discussed previously (Ref 10, 11) is that of a direct problem approach where dielectric response is estimated within the bounds of relatively well-defined

Table 7 Oscillation frequencies and IR intensities for four-molecule cluster of TNT

Frequency, cm^{-1}	Intensity, km/mol
6.0037	0.0276
6.8127	0.0135
9.5511	0.0445
10.7137	0.0363
13.1434	0.1926
14.6485	0.0858
17.4745	0.0361
19.1606	0.0969
21.5413	0.0717
25.5663	0.2335
27.2907	0.0672
28.3122	0.0329
32.3861	0.1016
34.9573	0.2077
40.7299	0.3467
45.9148	0.5988
50.9682	0.136
51.3221	0.1839
51.9382	0.6017
52.3798	0.3453
54.6865	0.0232
55.5157	0.0207
57.1434	0.358
62.0863	1.2134
67.9725	0.2731
73.8181	1.3738
82.7084	0.6903
91.401	0.4921
95.9635	1.9103
99.4256	0.6227
102.8424	1.2621
103.8391	9.4549
110.2973	5.5524
112.2823	14.0066
124.5235	5.1683
130.0222	1.9675
132.8818	2.7792
135.3963	1.4377
147.6898	2.1166
152.6375	5.3
153.1419	2.6393
157.2293	1.2297
165.0722	0.1527
175.0778	0.79
178.4232	1.1197
184.5245	1.3816
188.0139	2.7537
190.2879	0.3889
192.0548	3.329
192.7032	0.5122
196.8943	5.2073
198.2761	5.0334
199.7631	0.4605
202.1056	5.8742
294.9276	1.4559
296.7783	1.0261
297.8845	2.4338
298.8831	4.4941
324.7092	0.2389
325.209	0.6029
325.7378	0.148
325.811	0.0405
328.6621	0.7673
329.6841	0.4998

Table 7 Continued

Frequency, cm^{-1}	Intensity, km/mol
330.0564	0.8057
332.9135	0.1063
353.4549	2.2863
353.8611	2.0427
354.4024	2.9248
355.4821	3.7328
366.9194	1.0839
368.2383	1.9205
369.3088	3.9455
371.3992	4.807
384.9266	1.092
385.0972	1.1167
388.1738	0.4284
391.668	1.9364
463.06	0.3618
467.1603	1.1573
471.2585	0.2994
472.1674	1.6982
481.0948	0.1812
483.7679	0.597
484.3633	1.0706
485.0125	0.3554
540.766	2.8936
541.2985	1.5216
542.3571	0.716
542.7461	2.9325
549.0063	3.0966
549.4428	5.5645
550.4266	3.418
551.0865	2.0792
659.3755	11.1961
659.8872	3.4303
661.2794	13.0666
662.7278	9.7932
667.572	0.5246
669.3944	0.0793
672.8601	4.6511
673.2171	2.6274
716.6365	24.5244
716.9527	13.5797
718.0088	22.1708
719.3519	18.0592
739.063	24.7206
739.3708	130.8296
739.7837	7.1419
740.7033	70.2921
759.5333	23.6246
759.7645	42.8882
761.1715	20.4302
761.3542	30.9627
790.5221	0.8358
790.5998	0.8792
791.1676	2.192
791.3026	0.1507
795.9496	5.5813
796.7322	4.9704
797.4355	0.6989
797.6327	9.7116
805.0269	12.7807
805.3314	9.2942
806.0565	12.7468
807.2446	17.6478
842.8611	0.756
843.3628	3.0391
844.5015	1.8451

Table 7 Continued

Frequency, cm^{-1}	Intensity, km/mol
845.4727	2.1841
921.0493	17.8875
922.0851	40.7448
923.0247	45.2336
923.3955	28.3322
951.4396	6.7371
951.9678	39.1078
953.4363	32.0243
953.5462	24.8804
954.3428	34.9316
955.4679	4.9786
960.9208	3.5001
962.0534	9.2311
962.7248	8.0756
963.062	0.6791
966.6378	8.1237
968.2356	9.3892
1043.2646	8.177
1044.2894	6.1182
1048.3198	5.3386
1050.1333	2.0496
1050.6147	3.5367
1050.6708	3.3637
1052.1492	5.8976
1052.735	4.1214
1096.455	75.916
1096.6624	54.0083
1097.9261	37.4622
1100.058	41.0888
1185.3416	7.8041
1185.6052	16.1508
1185.7306	10.7674
1186.6664	12.6373
1209.8322	15.0783
1212.8856	15.3057
1214.3346	13.1397
1217.5505	16.2261
1219.2219	0.5039
1222.7281	10.706
1222.955	1.1508
1223.564	1.0288
1351.2896	9.5548
1353.3455	4.2628
1354.8254	5.0704
1355.7509	6.9006
1387.3927	504.0168
1388.4775	243.7943
1388.7524	87.4017
1389.0958	447.19
1392.4327	798.6592
1393.287	243.6454
1394.8691	156.6218
1396.2841	238.8504
1402.8853	40.1082
1405.0447	2.3998
1405.257	35.9898
1408.3396	49.7168
1419.1819	11.4361
1419.2982	4.5842
1420.2479	5.2822
1420.9575	11.7015
1424.3171	6.9025
1424.7	14.2952
1425.6173	3.7006
1426.0646	3.5978

Table 7 Continued

Frequency, cm^{-1}	Intensity, km/mol
1473.5498	9.0424
1474.6635	12.8272
1475.9045	16.0343
1476.1462	5.7658
1476.3361	10.2827
1477.5513	3.2443
1477.8824	21.6264
1478.4861	10.8031
1494.5078	2.0778
1497.4508	11.3855
1499.9305	5.7411
1499.9749	6.4007
1602.7976	89.5147
1604.576	75.0732
1605.7961	16.9799
1606.5385	136.8389
1614.0665	33.3701
1615.7209	24.6628
1617.3809	316.2843
1623.7596	58.5519
1624.993	121.0073
1630.8451	12.1011
1632.7219	102.004
1634.2406	2.0151
1659.2784	20.6782
1660.0342	35.6986
1663.2992	146.911
1664.3833	383.5529
1666.8501	298.8433
1668.7557	154.036
1669.1105	13.3956
1669.4171	381.2602
3073.4512	2.0504
3075.5383	0.5901
3076.5342	0.1196
3076.7654	0.9591
3143.1304	3.4185
3149.0393	8.8789
3149.7698	4.0967
3152.1172	3.5304
3177.7893	3.8554
3182.9602	2.5709
3190.4402	3.017
3204.1228	1.4827
3231.541	99.6425
3253.373	20.5025
3255.3308	23.642
3255.5933	23.5913
3256.0857	22.1997
3257.0527	24.6223
3258.084	18.7786
3265.4907	18.7129

adjustable parameters. Following this approach, a permittivity function is constructed using the DFT-calculated absorption spectra under the condition that the calculated resonance locations are fixed, while resonance widths and number densities are assumed adjustable. With respect to this approach, reference is again made to Fig. 5, 6, and 13-15, which show continuous spectra consisting of a superposition of essentially Lorenzian functions of various heights and widths, constructed using discrete spectra. Although the primarily purpose of this type of construction within GAUSSIAN is for the purpose of

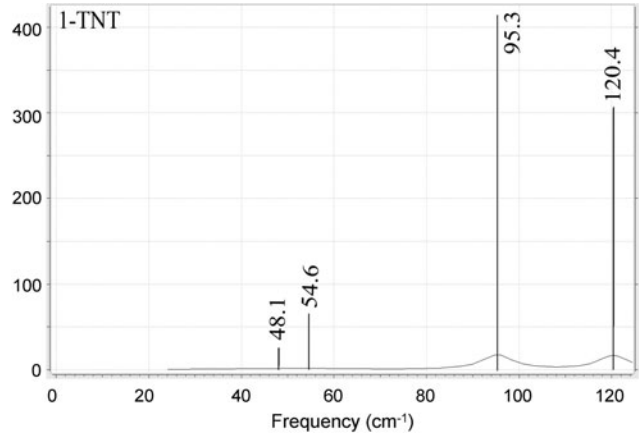

Fig. 10 IR intensity (arbitrary units) as a function of frequency calculated using DFT B3LYP/6-311G(2d,2p) for single isolated molecule of TNT according to frozen phonon approximation

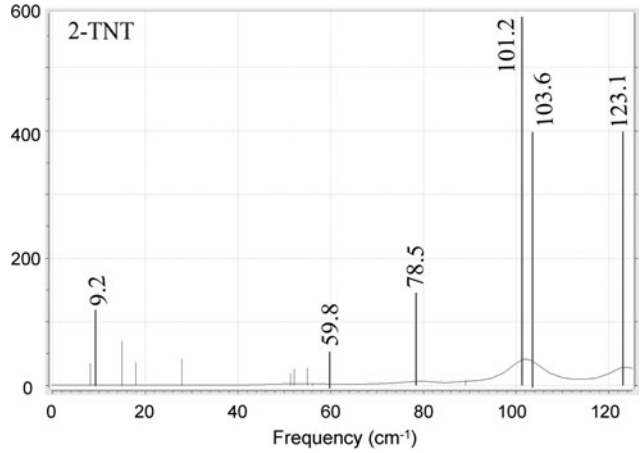

Fig. 11 IR intensity (arbitrary units) as a function of frequency calculated using DFT B3LYP/6-311G(2d,2p) for two-molecule cluster of TNT according to frozen phonon approximation

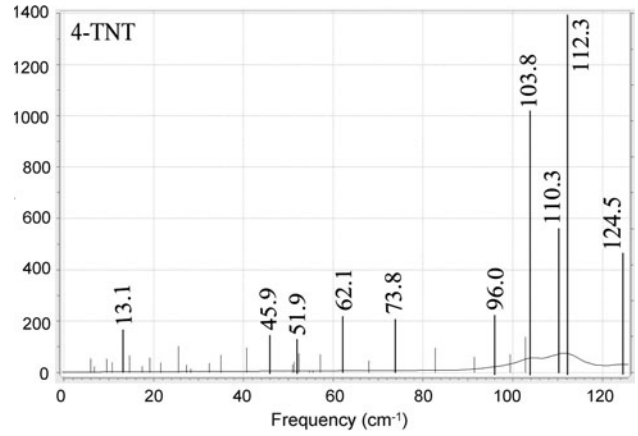

Fig. 12 IR intensity (arbitrary units) as a function of frequency calculated using DFT B3LYP/6-311G(2d,2p) for four-molecule cluster of TNT according to frozen phonon approximation

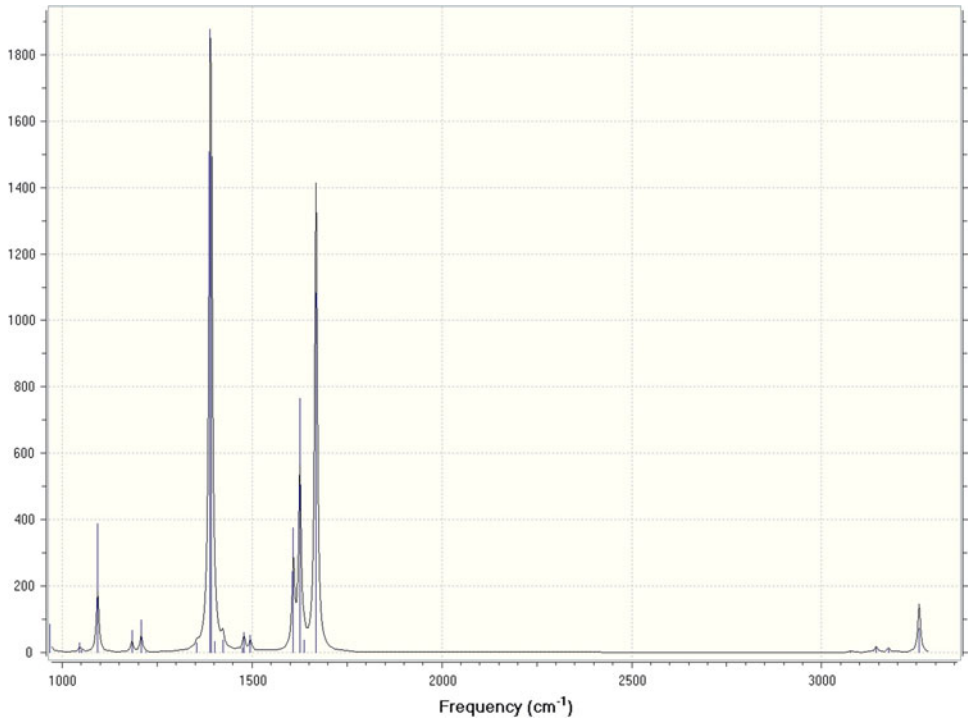

Fig. 13 Continuous-spectrum representation of IR intensity (arbitrary units) as a function of frequency calculated using DFT for single isolated molecule of TNT

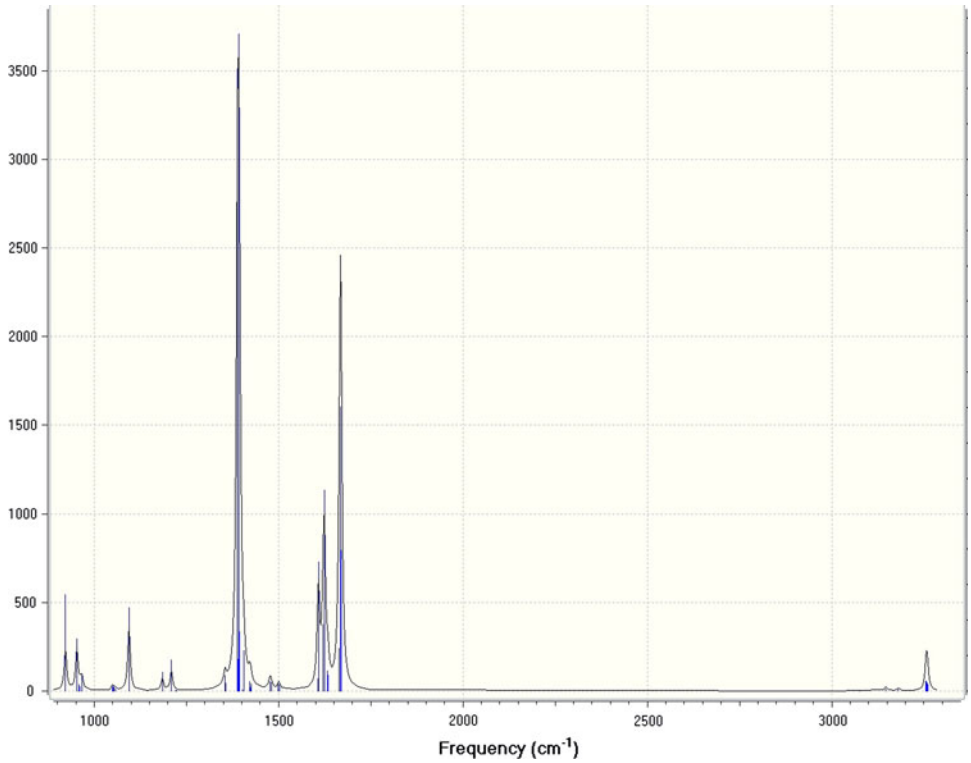

Fig. 14 Continuous-spectrum representation of IR intensity (arbitrary units) as a function of frequency calculated using DFT for two-molecule cluster of TNT

enhanced visualization of spectral features, it is significant to note that this operation represents, at some level, a zeroth-order estimation of the characteristic scaling and widths of resonances contributing to the dielectric response, i.e., permittivity function. For qualitative comparison of spectral features, this type of zeroth-order estimate should be sufficient. For the

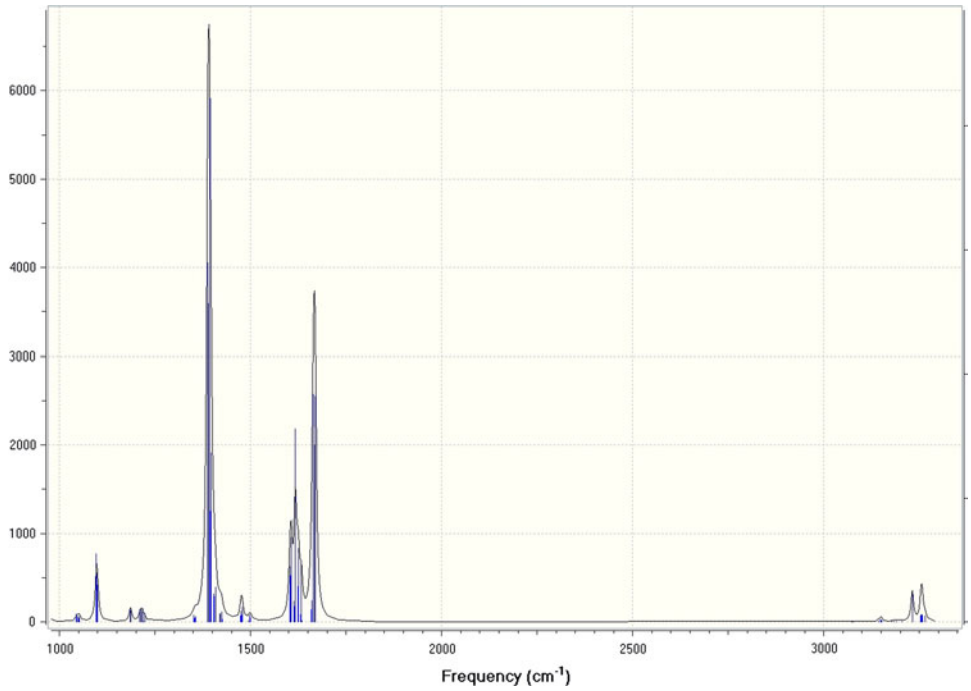

Fig. 15 Continuous-spectrum representation of IR intensity (arbitrary units) as a function of frequency calculated using DFT for four-molecule cluster of TNT

construction of permittivity functions to be used for quantitative simulations, it is more appropriate, however, to assume the characteristic scaling and widths of DFT-calculated resonances as adjustable parameters, i.e., parameters to be assigned values according to additional information.

Following an approach for construction of permittivity functions using DFT, which assumes the characteristic scaling and widths of resonances as adjustable parameters, inverse methods of analysis can be adopted. Accordingly, permittivity functions can be constructed using bin-averaged DFT-calculated spectra. Given the bin-averaged DFT spectra, permittivity function can be constructed using superpositions of Lorenzian functions that are in terms of reduced sets of phenomenological scaling and widths of resonances. This approach should consider, in principle, the sensitivity of reflectivity, as would be measured by a specific detection design (see Ref 9), with respect to level of bin averaging and variation in values of the associated phenomenological scaling and widths of resonances.

As demonstrated in this study, with respect to DFT calculations concerning molecular clusters, it is important to note that the atomic positions of the relaxed or equilibrium configuration of a single isolated molecule, e.g., Table 1 and 4, provide a convenient starting point. Accordingly, calculation of the dielectric response of molecular clusters that would represent an approximation of a bulk system entails the construction of a super cell consisting of molecules initial positions of which are those determined by DFT for isolated systems. Additional constraints on this super cell are based on crystallographic information concerning bulk density or lattice spacing.

It must be emphasized again in this study that, as in previous studies (Ref 10, 11), one purpose of DFT-calculated spectra, related to practical application and extremely important for interpretation signature features and the design of detectors, is the quantitative analysis of the inherent limitation on levels of detection associated with various types of detection strategies. With respect to the purpose of examining inherent limitations on IED detection, the dominant features of response spectra that are calculated using DFT provide a foundation for establishing what level of detection is achievable in the absence of instrumental and environmental factors associated with detection. Accordingly, the approach presented here, for construction of permittivity functions, provides a specific application of DFT. For any given energetic material and frequency range of the incident electromagnetic wave, DFT can calculate a set of response signatures each of which is characterized by an excitation frequency, magnitude, and width. These response signatures must then be adjusted parametrically to construct permittivity functions. Accordingly, parameter adjustment with respect to a given set of experimental measurements, which would entail parameter optimization and sensitivity analysis, will determine what types of signature structure are recoverable at the level of detection for a given detector design.

Finally, the DFT calculations presented here were performed using the DFT software GAUSSIAN. With respect to the approach presented here for the construction of permittivity functions, these calculations represent results of numerical experiments with the "numerical apparatus" GAUSSIAN, which has associated with it specific discrete numerical representations and associated approximations. Again, an underlying factor supporting the construction of permittivity functions using DFT-calculated spectra is that the associated software technology has evolved to a point of maturity where dielectric response to electromagnetic excitation can be determined quantitatively for large molecular systems.

6. Conclusion

The calculations of ground state resonance structure associated with molecular clusters of PETN and TNT using DFT are meant to serve as reasonable estimates of molecular level response characteristics, providing interpretation of dielectric response features, for subsequent adjustment relative to experimental measurements and additional constraint based on molecular structure theory. With respect to spectroscopic methods for the detection of explosives, i.e., different types of detection strategies and their associated algorithms for post-processing of measurements, the calculated resonance spectra presented here serve the purpose of simulating detector designs for detection of molecular clusters of explosives. That is to say, for detection of spatially distributed molecular clusters of explosives, these spectra can be assumed as a reasonable estimate of dielectric response for purposes of the practical detection. In addition, it must be remembered that many types of explosives existing in bulk should not be assumed to have microstructure or dielectric response characteristics corresponding to a lattice. In many cases, explosives in bulk are characterized by molecular clusters, which are distributed within a host or binder material. For these cases, it is reasonable to assume that, as demonstrated in this study, many of the dielectric response characteristics of small molecular clusters, as well as isolated molecules remain preserved. This follows in that molecule-molecule coupling in these cases is more characteristic of isolated scattering sites, rather than that of a lattice structure.

Acknowledgment

This study was supported by the Office of Naval Research.

References

1. B.M. Rice and C.F. Chabalowski, Ab Initio and Nonlocal Density Functional Study of 1,3,5-Trinitro-*s*-triazine (RDX) Conformers, *J. Phys. Chem.*, 1997, **101**, p 8720
2. Y. Chen, H. Liu, Y. Deng, D. Schauki, M.J. Fitch, R. Osiander, C. Dodson, J.B. Spicer, M. Shur, and X.-C. Zhang, THz Spectroscopic Investigation of 2,4-dinitrotoluene, *Chem. Phys. Lett.*, 2004, **400**, p 357–361
3. D.G. Allis, D.A. Prokhorova, and T.M. Korter, Solid-State Modeling of the Terahertz Spectrum of the High Explosive HMX, *J. Phys. Chem. A*, 2006, **110**, p 1951–1959
4. D.G. Allis and T.M. Korter, Theoretical Analysis of the Terahertz Spectrum of the High Explosive PETN, *Chem. Phys. Chem.*, 2006, **7**, p 2398
5. J. Chen, Y. Chen, H. Zhao, G.J. Bastiaans, and X.-C. Zhang, *Opt. Exp.*, 2007, **15**, p 11763
6. M.R. Leahy-Hoppa, M.J. Fitch, X. Zheng, L.M. Hayden, and R. Osiander, Wideband Terahertz Spectroscopy of Explosives, *Chem. Phys. Lett.*, 2007, **434**, p 227–230
7. J. Hooper, E. Mitchell, C. Konek, and J. Wilkinson, Terahertz Spectroscopy Techniques for Explosives Detection, *Chem. Phys. Lett.*, 2009, **467**, p 309
8. M.R. Leahy-Hoppa, M.J. Fitch, and R. Osiander, Terahertz Spectroscopy Techniques for Explosives Detection, *Anal. Bioanal. Chem.*, 2009, **395**, p 247
9. A. Shabaev, S.G. Lambrakos, N. Bernstein, V.L. Jacobs, and D. Finkenstadt, A General Framework for Numerical Simulation of Improvised Explosive Device (IED)-Detection Scenarios Using Density Functional Theory (DFT) and Terahertz (THz) Spectra, *Appl. Spectrosc.*, 2011, **65**, p 409
10. A. Shabaev, S.G. Lambrakos, N. Bernstein, V. Jacobs, and D. Finkenstadt, THz Dielectric Properties of High Explosives Calculated by Density Functional Theory for the Design of Detectors, *J. Mater. Eng. Perform.*, 2011, **20**(9), p 1536
11. L. Huang, A. Shabaev, S.G. Lambrakos, N. Bernstein, V. Jacobs, D. Finkenstadt, and L. Massa, Dielectric Response of High Explosives at THz Frequencies Calculated Using Density Functional Theory, *J. Mater. Eng. Perform.*, 2011, doi:10.1007/s11665-011-0020-3
12. M.J. Frisch, G.W. Trucks, H.B. Schlegel, G.E. Scuseria, M.A. Robb, J.R. Cheeseman, G. Scalmani, V. Barone, B. Mennucci, G.A. Petersson, H. Nakatsuji, M. Caricato, X. Li, H.P. Hratchian, A.F. Izmaylov, J. Bloino, G. Zheng, J.L. Sonnenberg, M. Hada, M. Ehara, K. Toyota, R. Fukuda, J. Hasegawa, M. Ishida, T. Nakajima, Y. Honda, O. Kitao, H. Nakai, T. Vreven, J.A. Montgomery, Jr., J.E. Peralta, F. Ogliaro, M. Bearpark, J.J. Heyd, E. Brothers, K.N. Kudin, V.N. Staroverov, R. Kobayashi, J. Normand, K. Raghavachari, A. Rendell, J.C. Burant, S.S. Iyengar, J. Tomasi, M. Cossi, N. Rega, J.M. Millam, M. Klene, J.E. Knox, J.B. Cross, V. Bakken, C. Adamo, J. Jaramillo, R. Gomperts, R.E. Stratmann, O. Yazyev, A.J. Austin, R. Cammi, C. Pomelli, J.W. Ochterski, R.L. Martin, K. Morokuma, V.G. Zakrzewski, G.A. Voth, P. Salvador, J.J. Dannenberg, S. Dapprich, A.D. Daniels, Ö. Farkas, J.B. Foresman, J.V. Ortiz, J. Cioslowski, and D.J. Fox, *Gaussian 09, Revision A.1*, Gaussian, Inc., Wallingford, CT, 2009
13. A. Frisch, M.J. Frisch, F.R. Clemente, and G.W. Trucks, *Gaussian 09 User's Reference*, Gaussian Inc., 2009, p 105–106, online: www.gaussian.com/g_tech/g_ur/g09help.htm
14. P. Hohenberg and W. Kohn, Inhomogeneous Electron Gas, *Phys. Rev.*, 1964, **136**, p B864
15. W. Kohn and L.J. Sham, Self-Consistent Equations Including Exchange and Correlation Effects, *Phys. Rev.*, 1965, **140**, p A1133
16. R.O. Jones and O. Gunnarson, The Density Functional Formalism, Its Applications and Prospects, *Rev. Mod. Phys.*, 1989, **61**, p 689
17. W.W. Hager and H. Zhang, A Survey of Nonlinear Conjugate Gradient Methods, *Pac. J. Optim.*, 2006, **2**, p 35–58
18. R.M. Martin, *Electronic Structures Basic Theory and Practical Methods*, Cambridge University Press, Cambridge, 2004, p 25
19. E.B. Wilson, J.C. Decius, and P.C. Cross, *Molecular Vibrations*, McGraw-Hill, New York, 1955
20. J.W. Ochterski, *Vibrational Analysis in Gaussian*, help@gaussian.com, 1999
21. C.A.D. Roeser and E. Mazur, Light-Matter Interactions on Femtosecond Time Scale, *Frontiers of Optical Spectroscopy. NATO Science Series*, Vol 168, B. Di Bartolo and O. Forte, Ed., Kluwer Academic Publishers, Dordrecht, 2005, p 29
22. C.F. Bohren and D.R. Huffman, *Absorption and Scattering of Light by Small Particles*, Wiley-VCH Verlag, Weinheim, 2004
23. A.D. Becke, Density-functional Thermochemistry. III. The Role of Exact Exchange, *J. Chem. Phys.*, 1993, **98**, p 5648–5652
24. B. Miehlich, A. Savin, H. Stoll, and H. Preuss, Results Obtained with the Correlation Energy Density Functionals of Becke and Lee, Yang and Parr, *Chem. Phys. Lett.*, 1989, **157**, p 200–206
25. A.D. McLean and G.S. Chandler, Contracted Gaussian-Basis Sets for Molecular Calculations. 1. 2nd row atoms, $Z = 11$-18, *J. Chem. Phys.*, 1980, **72**, p 5639–5648
26. T. Clark, J. Chandrasekhar, G.W. Spitznagel, and P.V.R. Schleyer, Efficient Diffuse Function-Augmented Basis-Sets for Anion Calculations. 3. The 3-21+G Basis Set for 1st-Row Elements, Li-F, *J. Comp. Chem.*, 1983, **4**, p 294–301
27. M.J. Frisch, J.A. Pople, and J.S. Binkley, Self-Consistent Molecular Orbital Methods. 25. Supplementary Functions for Gaussian Basis Sets, *J. Chem. Phys.*, 1984, **80**, p 3265–3269
28. I.J. Bruno, J.C. Cole, P.R. Edgington, M.K. Kessler, C.F. Macrae, P. McCabe, J. Pearson, and R. Taylor, New Software for Searching the Cambridge Structural Database and Visualizing Crystal Structures, *Acta Cryst.*, 2002, **B58**, p 389–397